Pre-print version

Final Article published in:

Numerical Heat Transfer, Part A, 49: 733–763, 2006
ISSN: 1040-7782 print=1521-0634 online
DOI: 10.1080/10407780500503854

COUPLED HEAT AND MOISTURE TRANSPORT IN CONCRETE AT ELEVATED TEMPERATURES - EFFECTS OF CAPILLARY PRESSURE AND ADSORBED WATER

Colin T. Davie[†], Chris J. Pearce[‡] and Nenad Bićanić[‡]

[†]School of Civil Engineering and Geosciences, University of Newcastle

[‡]Department of Civil Engineering, University of Glasgow

Mailing Address:

School of Civil Engineering and Geosciences

School Office: Drummond Building

University of Newcastle

Newcastle upon Tyne

NE1 7RU

UK

Abbreviated Title:

COUPLED HEAT AND MOISTURE TRANSPORT IN CONCRETE

Abstract

The importance of capillary pressure and adsorbed water in the behaviour of heat and moisture transport in concrete exposed to high temperatures is explored by incorporating their behaviour explicitly into a computational model. The inclusion of these two phenomena is realised with a formulation of a modified model, which represents an extension to the significant work of Tenchev et al. Comparative studies were carried out, using a benchmark problem, and it was determined that, while the Tenchev formulation under estimated the capacity for fluid transport in the concrete resulting in an over prediction of pore pressures (which may affect the prediction of mechanical damage and spalling), the inclusion of capillary pressure had little effect on the results. More important was the accurate representation of the free water flux, which has a significant effect on the prediction of vapour content and subsequently pore pressure. It was furthermore found that, while the adsorbed water flux may be minimal when concrete is exposed to high temperature, its presence has a significant effect on the fluid transport behaviour and the prediction of pore pressures.

Nomenclature

C_i - specific heat of phase i (for $i = A, L, S, V$)

D_i - diffusion coefficient of Dry Air in Water Vapour (i=AV) or Water Vapour in Dry Air (i=VA) within the porous concrete

D_B - diffusion coefficient of adsorbed water

e - emissivity

$\dot{E}_{FW}$ - rate of evaporation (including desorbtion)

h_q - convective heat transfer coefficient on boundary

h_r - radiative heat transfer coefficient on boundary

h_{qr} - combined heat transfer coefficient on boundary

$\mathbf{J}_i$ - mass flux of a phase i (for $i = A, G, L, V$)

K - intrinsic permeability of the dry concrete

k - thermal conductivity of concrete

K_i - relative permeability of phase i (for $i = G, L$)

P_i - partial pressure of phase i (for $i = A, G, L, V$)

P_C - capillary pressure

P_{Pore} - averaged fluid pressure in pore space

P_{Sat} - saturation pressure of water

R_i - gas constant for phase i (for $i = A, V$)

S - degree of saturation with free water

S_B - degree of saturation adsorbed water

S_{SSP} - solid saturation point

T - absolute temperature (°K)

T_C - temperature (°C)

t - time

$\mathbf{v}_i$ - component of velocity of phase i (for $i = B, G, L$)

α_{Air} - thermal diffusivity of dry air

β - coefficient of water vapour mass transfer on boundary

δ - concrete constrictivity factor

ε_i - volume fraction of phase i (for $i = A, D, G, L, S, V$)

ϕ - porosity

λ_D - specific heat of dehydration

λ_E - specific heat of evaporation

μ_i - dynamic viscosity of phase i (for $i = A, G, L, V$)

$\underline{\rho C}$ - heat capacity of concrete

$(\rho C)_{Air}$ - heat capacity of dry air

$\underline{\rho C \mathbf{v}}$ - energy transferred by fluid flow, i.e. convection

ρ_i - density of a phase i (for $i = Cem, L, S$)

$\tilde{\rho}_i$ - mass of a phase i per unit volume of gaseous material (for $i = A, G, V$)

τ - concrete tortuosity factor

Subscripts

A - dry air phase

B - physically bound, adsorbed water

C - capillary

Cem - cement

D - chemically bound water released by dehydration

FW - free (combined liquid and adsorbed) water

G - gas phase

L - liquid water phase

M - moisture, (free water and water vapour phases)

S - solid phase

V - water vapour phase

∞ - atmospheric conditions beyond the boundary

1. Introduction and Scope

Although, for many years concrete has been one of the most widely used and well understood construction materials, in the light of recent extreme events, including accidents, arson and terrorism, its performance when exposed to high temperature has come to the forefront of interest for both industry and research. These events and recent research work have highlighted the lack of a full understanding of how concrete behaves under rapid thermal loading. For example, the Channel Tunnel fire in 1996 illustrated the structural, safety and economic consequences of a 10-hour fire that reached temperatures of 700°C, when thermal spalling of the concrete liner resulted in severe structural damage over a significant length of the tunnel [1]. After subsequent investigations, no real consensus emerged as to the exact mechanisms underlying the observed spalling phenomenon.

However, full consensus exists that the behaviour of concrete under exposure to high temperatures is greatly dependent on its composite structure and in particular on the physical and chemical composition of the cement paste. The hardened cement paste is a highly porous, hygroscopic material, the volume of which comprises approximately 28% gel pores (i.e. pores $\leq$ 2.6nm in diameter) and up to 40% capillary pores (i.e. pores in the range of 1μm in diameter) [2]. At room temperature, the pores may be fully or partially filled with fluids typically including liquid water, water vapour and dry air. Furthermore, within the gel pores and on the surfaces of the capillary pores, the water exists as adsorbed water, physically bound to the solid, and as such does not behave as a liquid. The solid skeleton of the paste itself is composed of various chemical compounds and chemically bound water.

When exposed to high temperature, heat is conducted and convected through the material, resulting in changes in the chemical composition, physical structure and fluid content of the cement paste which in turn affect the overall mechanical (strength, stiffness, fracture energy, etc.) and other physical properties (thermal conductivity, permeability, porosity, etc.) of the concrete.

In order to construct an appropriate mathematical model for concrete subject to thermal loading all of these (mostly non-linear) phenomena and their coupled interactions must be considered. Such a model is therefore very complex. To model the changes in fluid content alone, both pressure driven flow and diffusion must be considered for all fluids present, along with evaporation and

condensation phase changes. Despite these difficulties, much work has previously been conducted in this area and several models have been developed, including important contributions by Coussy [3], Gawin et al. [4] and Lewis & Schrefler [5].

The starting point for this work represents a significant, albeit less well known, model for the coupled transfer of heat and moisture in concrete clearly elucidated in Tenchev et al. [6] and formulated in the context of coupled Finite Element analysis (subsequently referred to here as the Tenchev Model). This model, while quite comprehensive and fully generalised for 3-dimensional analysis, includes several assumptions and restrictions which warrant further attention, while excluding various phenomena that may be vital for a more detailed analysis of the transport phenomena within concrete exposed to high temperature. This work focuses on the treatment of two important aspects - capillary pressure phenomena and adsorbed water. These phenomena may be of particular relevance if the hygro-thermal model is also coupled with mechanical behaviour. Moreover this work will not consider any implications associated with other specific constitutive relationships employed in the original Tenchev Model.

As far as capillary pressure is concerned, the Tenchev Model is not completely consistent. The model assumes that the pressures of the liquid and gases contained in the pores, both of which have a significant influence on the fluid transport behaviour, are equal, i.e. $P_G = P_L$, at all times. Since capillary pressure is defined as, $P_C = P_G - P_L$, the difference between the gas and the liquid pressures, the statement $P_G = P_L$ is only physically correct when there is no capillary pressure. Moreover, following from the Kelvin Equation, the capillary pressure is also related to the relative humidity and, for thermodynamic equilibrium, the constraint $P_G = P_L$ implies a relative humidity of 100%. Since the relative humidity can vary considerably from 100% when concrete is exposed to high temperatures, P_L would vary considerably from P_G and it is uncertain to what extent the adopted constraint is a valid approximation. No further evidence or justification is given in [6] in support of this approximation.

Instead, in order to account for the effects of capillary pressure on the transport behaviour the Tenchev Model adopts a fixed relative permeability of the liquid phase, K_L=0.01. This is clearly not consistent with the previous assumptions discussed above since, while the reduction of K_L may to some extent simulate the reduction in transport that would be caused by capillary suction, the choice

of this particular value seems arbitrary and it is difficult to justify the fact that it is assumed constant when relative humidity, and therefore capillary pressure, is seen to vary.

Moreover, the Tenchev Model ignores the diffusion of adsorbed water on the assumption that its flux is negligible. Again no supporting statements are made and furthermore, no other behaviour relating to the presence of water in an adsorbed state rather than in liquid form is considered. Given the very large internal surface area of hardened cement paste (~500m^2 per cm^3 [7]) and its high gel pore content, a very large proportion (up to 50-60% at room temperature) of the free water content in the concrete exists as adsorbed water [4]. Therefore, although the flux may be low, the presence of adsorbed water can be a significant factor when considering the overall transport of moisture in concrete. Furthermore, as will be shown, this has implications for the evolution of capillary pressure.

Following a brief review of the Tenchev Model, a modified model is proposed which accounts explicitly for capillary pressure and part of the free water existing in an adsorbed state. The results of a Finite Element study of the effects of the phenomena described above on heat and moisture transfer in concrete subjected to high temperatures predicted by the Modified Model were then compared with those of the Tenchev Model. The aim was to determine the importance of capillary pressure and adsorbed water in the development of fluid transport behaviour in concrete exposed to intense heating, as well as to assess the adequacy of the modelling assumptions and constraints made in the Tenchev Model.

To ensure the validity of the study and that the effects on the results were solely related to the modified consideration of capillary pressure and adsorbed water, all other constituent parts of the Modified Model, as well as the values of all material parameters and relationships, were unchanged compared those employed in the Tenchev Model.

2. Mathematical Model

In the following description of the model formulation, the nomenclature and style adopted by Tenchev et al. [6] have been followed as closely as possible and extended where required to include capillary pressure and adsorbed water effects. In order to allow for such generalisations, the subscript *L*, employed by Tenchev to represent liquid water, has been replaced where appropriate with *FW* to

signify free water, which consists of both liquid water and, in certain cases, adsorbed water. It may also be noted that, in order to allow complete freedom for model development, all phase contents are described in terms of volume fractions and densities, $\varepsilon_i \rho_i$, rather then the 'mass per volume concrete', $\overline{\rho}_i$, as used by Tenchev et al.

2.1. Conservation Equations

The governing mass conservation equations to describe heat and moisture transport in concrete containing free water, water vapour and dry air can be defined as follows (1)-(3):

$$\frac{\partial(\varepsilon_G \tilde{\rho}_V)}{\partial t} = -\nabla \cdot \mathbf{J}_V + \dot{E}_{FW} \tag{1}$$

$$\frac{\partial(\varepsilon_G \tilde{\rho}_A)}{\partial t} = -\nabla \cdot \mathbf{J}_A \tag{2}$$

$$\frac{\partial(\varepsilon_{FW} \rho_L)}{\partial t} = -\nabla \cdot \mathbf{J}_{FW} - \dot{E}_{FW} + \frac{\partial(\varepsilon_D \rho_L)}{\partial t} \tag{3}$$

where, ε_i is the volume fraction of a phase i, ρ_i is the density of a phase i, $\tilde{\rho}_i$ is the mass of a phase i per unit volume of gaseous material, $\mathbf{J}_i$ is the mass flux of a phase i, $\dot{E}_{FW}$ is rate of evaporation of free water (including desorbtion), t is time and i = *FW, V, A, D* are respectively free water, water vapour, dry air, and dehydrated water phases. It may be noted that the term describing the change in dehydrated water content is contained within the free water mass conservation equation (1) since chemically bound water is assumed to be initially released as liquid water.

The energy conservation for the system can be defined as:

$$\underline{(\rho C)}\frac{\partial T}{\partial t} = -\nabla \cdot (-k\nabla T) - \underline{(\rho C \mathbf{v})} \cdot \nabla T - \lambda_E \dot{E}_{FW} - \lambda_D \frac{\partial(\varepsilon_D \rho_L)}{\partial t} \tag{4}$$

where, $\underline{\rho C}$ is the heat capacity of concrete, k is the thermal conductivity of concrete, $\underline{\rho C \mathbf{v}}$ relates to the energy transferred by fluid flow, λ_E is the specific heat of evaporation (or of desorption when appropriate), λ_D is the specific heat of dehydration and T is the absolute temperature.

Equations (1)-(4) are rearranged, as shown below (5)-(7), to develop a system of three governing equations for dry air, moisture and energy conservation.

$$\frac{\partial(\varepsilon_G \tilde{\rho}_A)}{\partial t} = -\nabla \cdot \mathbf{J}_A \tag{5}$$

$$\frac{\partial(\varepsilon_G \tilde{\rho}_V)}{\partial t} + \frac{\partial(\varepsilon_{FW} \cdot \rho_L)}{\partial t} - \frac{\partial(\varepsilon_D \rho_L)}{\partial t} = -\nabla \cdot (\mathbf{J}_V + \mathbf{J}_{FW}) \tag{6}$$

$$(\underline{\rho C})\frac{\partial T}{\partial t} - \lambda_E \frac{\partial(\varepsilon_{FW} \cdot \rho_L)}{\partial t} + (\lambda_D + \lambda_E)\frac{\partial(\varepsilon_D \rho_L)}{\partial t} = \nabla \cdot (k \nabla T) + \lambda_E \nabla \cdot \mathbf{J}_{FW} - (\underline{\rho C \mathbf{v}}) \cdot \nabla T \tag{7}$$

This formulation (1)-(7) is identical to that derived by Tenchev et al. [6], and is employed, unchanged for all models discussed in the following sections.

2.2. Original Formulation of the Tenchev Model [6]

Constitutive Laws

This section reviews the constitutive laws derived for the Tenchev Model using the notation adopted in this work. The mass fluxes of dry air, water vapour and free water can be expressed in terms of pressure and concentration gradients assuming that Darcy's and Fick's laws are applicable and that the diffusion of adsorbed water on the surface of the solid cement paste skeleton is negligible (8)-(10).

$$\mathbf{J}_A = \varepsilon_G \tilde{\rho}_A \mathbf{v}_G - \varepsilon_G \tilde{\rho}_G D_{AV} \nabla\left(\frac{\tilde{\rho}_A}{\tilde{\rho}_G}\right) \tag{8}$$

$$\mathbf{J}_V = \varepsilon_G \tilde{\rho}_V \mathbf{v}_G - \varepsilon_G \tilde{\rho}_G D_{VA} \nabla\left(\frac{\tilde{\rho}_V}{\tilde{\rho}_G}\right) \tag{9}$$

$$\mathbf{J}_{FW} = \varepsilon_{FW} \rho_L \mathbf{v}_L \tag{10}$$

where, D_{AV} and D_{VA} are respectively the diffusion coefficients of dry air in water vapour and water vapour in dry air within the porous concrete (which are subsequently assumed to be equal [8]), and $\mathbf{v}_G$ and $\mathbf{v}_L$ are the velocities of the gas and liquid water phases resulting from pressure driven flow as given below by Darcy's law (11) & (12)

$$\mathbf{v}_G = -\frac{KK_G}{\mu_G} \nabla P_G \tag{11}$$

$$\mathbf{v}_L = -\frac{KK_L}{\mu_L} \nabla P_L \tag{12}$$

where, K is the intrinsic permeability of the dry concrete, K_G & K_L are the relative permeabilities of the gas and liquid phases, μ_G & μ_L are their dynamic viscosities and P_G & P_L are the corresponding

pressures. As described earlier, for simplicity, the liquid pressure is, by Tenchev et al., assumed to be equal to the gas pressure, $P_G = P_L$ (see discussion regarding capillary pressure in the introduction), and thus, equation (12) may be rewritten as:

$$\mathbf{v}_L = -\frac{KK_L}{\mu_L}\nabla P_G \tag{12a}$$

The dry air and water vapour are assumed to behave as ideal gases (13) and their pressures and partial densities are considered to be additive as defined by Dalton's law [8] (14):

$$P_A = R_A\tilde{\rho}_A T \qquad P_V = R_V\tilde{\rho}_V T \tag{13}$$

$$P_G = P_A + P_V \qquad \tilde{\rho}_G = \tilde{\rho}_A + \tilde{\rho}_V \tag{14}$$

where, P_A & P_V are the pressures and R_A & R_V the gas constants of the dry air and water vapour [8].

For temperatures below the critical point of water (374.14°C), the volume fraction of free water in the concrete is determined from Sorption Isotherms, as defined by Bažant and Kaplan [9], which relate the free water content to the cement content of the concrete and the relative humidity and temperature in the pores (15).

$$\varepsilon_{FW} = \frac{\varepsilon_{Cem}\rho_{Cem}}{\rho_L}\cdot f\left(\frac{P_V}{P_{Sat}}, T\right) \tag{15}$$

where, $\varepsilon_{Cem}\rho_{Cem}$ is the cement content per unit volume of concrete, P_{Sat} is the saturation pressure of water vapour and (P_V /P_{Sat}) is the relative humidity (See AI.33 in Appendix I). For temperatures above the critical point for water, where liquid water cannot exist, P_{Sat} is undefined, and the free water content is taken as zero.

The gas volume fraction can then be determined from equation (16) below:

$$\phi = \varepsilon_{FW} + \varepsilon_G \tag{16}$$

where, ϕ is the concrete porosity.

Finally, the term describing energy transport by fluid flow ($\underline{\left(\rho C\mathbf{v}\right)}\cdot\nabla T$ in (7)) is neglected since it is assumed that the transfer of energy by convection is accounted for within the relationship for the thermal conductivity of concrete, k, which has been determined empirically for wet concrete.

In addition to the thermal conductivity, k, there are further parameters that occur in the above formulation which are interdependent and typically functions of temperature. The specific

relationships used both in this work, as well as in Tenchev et al. [6], are listed in full in Appendix I. While it is clear that some of these may be considered oversimplified, the specific nature of the relationships employed does not affect the overall formulation of the models and it does not affect the model extension which will be introduced in Section 2.3. It is however noted that certain physical parameters critical to the transport behaviour, such as the intrinsic permeability and porosity of the concrete, as well as the proportional volumes of chemically bound water, free water and water vapour, are heavily interrelated and furthermore that they are strongly dependent on the initial water/cement ratio of the concrete mix. In that context, it is not certain whether the values of the parameters employed by Tenchev et al. [6] were fully consistent with one another or with a particular water/cement ratio. Nonetheless, in order to conduct a valid comparison of the suggested modification with the original Tenchev Model the same reported parameters and values were utilised. It was therefore tacitly assumed that the values and temperature dependent formulations for porosity, ϕ, intrinsic permeability, K, and the saturation free water content†, ${\varepsilon_{FW}}^0{\rho_L}^0$, were consistent for the concrete under investigation.

Numerical Model - Differential Equations

From the governing equations (5)-(7) a system of coupled differential equations can be developed, with reference to an appropriate choice of primary variables, leading to (17):

$$\mathbf{C}\dot{\mathbf{u}} - \nabla\cdot\left(\mathbf{K}\nabla\mathbf{u}\right) = 0 \tag{17}$$

The chosen set of primary variables in the Tenchev Model was (18):

$$\mathbf{u} = \begin{pmatrix} T & P_G & \tilde{\rho}_V \end{pmatrix}^{\mathrm{T}} \tag{18}$$

After extensive algebraic manipulation, the system of governing differential equations can be written in the form below (19)-(21).

$$C_{TT}\frac{\partial T}{\partial t} + C_{TP}\frac{\partial P_G}{\partial t} + C_{TV}\frac{\partial \tilde{\rho}_V}{\partial t} = \nabla\cdot\left(K_{TT}\nabla T + K_{TP}\nabla P_G + K_{TV}\nabla\tilde{\rho}_V\right) \tag{19}$$

$$C_{AT}\frac{\partial T}{\partial t} + C_{AP}\frac{\partial P_G}{\partial t} + C_{AV}\frac{\partial \tilde{\rho}_V}{\partial t} = \nabla\cdot\left(K_{AT}\nabla T + K_{AP}\nabla P_G + K_{AV}\nabla\tilde{\rho}_V\right) \tag{20}$$

† The saturation free water content, referred to by Tenchev et al. as the 'initial water content', represents the free water content in the concrete when thermodynamic equilibrium is reached at 100% relative humidity. It is used in the model formulation to define Bažant's Sorption Isotherms (See equations (15) and (AI.33)).

$$C_{MT}\frac{\partial T}{\partial t}+C_{MP}\frac{\partial P_G}{\partial t}+C_{MV}\frac{\partial \tilde{\rho}_V}{\partial t}=\nabla\cdot\left(K_{MT}\nabla T+K_{MP}\nabla P_G+K_{MV}\nabla\tilde{\rho}_V\right) \tag{21}$$

where,

$$C_{TT}=\left(\underline{\rho C}\right)+\left(\lambda_D+\lambda_E\right)\left(\varepsilon_D\frac{\partial\rho_L}{\partial T}+\rho_L\frac{\partial\varepsilon_D}{\partial T}\right)-\lambda_E\left(\varepsilon_L\frac{\partial\rho_L}{\partial T}+\rho_L\frac{\partial\varepsilon_{FW}}{\partial T}\right);\quad C_{TP}=0;\quad C_{TV}=-\lambda_E\rho_L\frac{\partial\varepsilon_{FW}}{\partial\tilde{\rho}_V} \tag{22}$$

$$C_{AT}=\tilde{\rho}_A\left(\frac{\partial\phi}{\partial T}-\frac{\partial\varepsilon_{FW}}{\partial T}\right)-\frac{\varepsilon_G P_G}{R_A T^2};\qquad C_{AP}=\frac{\varepsilon_G}{R_A T};\qquad C_{AV}=-\frac{\varepsilon_G R_V}{R_A}-\tilde{\rho}_A\frac{\partial\varepsilon_{FW}}{\partial\tilde{\rho}_V} \tag{23}$$

$$C_{MT}=\tilde{\rho}_V\frac{\partial\phi}{\partial T}+\left(\varepsilon_{FW}-\varepsilon_D\right)\frac{\partial\rho_L}{\partial T}+\left(\rho_L-\tilde{\rho}_V\right)\frac{\partial\varepsilon_{FW}}{\partial T}-\rho_L\frac{\partial\varepsilon_D}{\partial T};\quad C_{MP}=0;\quad C_{MV}=\varepsilon_G+\left(\rho_L-\tilde{\rho}_V\right)\frac{\partial\varepsilon_{FW}}{\partial\tilde{\rho}_V} \tag{24}$$

$$K_{TT}=k;\qquad K_{TP}=-\lambda_E\varepsilon_{FW}\rho_L\frac{KK_L}{\mu_L};\qquad K_{TV}=0 \tag{25}$$

$$K_{AT}=-\frac{\varepsilon_G D_{AV}\tilde{\rho}_V P_G}{\tilde{\rho}_G R_A T^2};\qquad K_{AP}=\frac{KK_G}{\mu_G}\varepsilon_G\tilde{\rho}_A+\frac{\varepsilon_G D_{AV}\tilde{\rho}_V}{\tilde{\rho}_G R_A T};\qquad K_{AV}=-\frac{\varepsilon_G D_{AV}}{\tilde{\rho}_G}\left(\tilde{\rho}_A+\frac{R_V}{R_A}\tilde{\rho}_V\right) \tag{26}$$

$$K_{MT}=\frac{\varepsilon_G D_{AV}\tilde{\rho}_V P_G}{\tilde{\rho}_G R_A T^2};\quad K_{MP}=\frac{KK_G}{\mu_G}\varepsilon_G\tilde{\rho}_V-\frac{\varepsilon_G D_{AV}\tilde{\rho}_V}{\tilde{\rho}_G R_A T}+\varepsilon_{FW}\rho_L\frac{KK_L}{\mu_L};\quad K_{MV}=\frac{\varepsilon_G D_{AV}}{\tilde{\rho}_G}\left(\tilde{\rho}_A+\frac{R_V}{R_A}\tilde{\rho}_V\right) \tag{27}$$

These differential equations can then be solved using a standard finite element formulation as described in the sections below. It should be noted that fundamental to the formulation given above are the assumptions that the diffusion of dry air in water vapour is equal to the diffusion of water vapour in dry air, $D_{AV} = D_{VA}$, and that the liquid pressure is equal to gas pressure, $P_L = P_G$. Full derivations for all of the matrix components can be found in the original paper by Tenchev et al. [6].

2.3. Extended Formulation - The Modified Model

Constitutive Laws

As discussed earlier, the formulation for the Tenchev Model is here modified and extended in order to explicitly consider two potentially significant effects - capillary pressure and physically bound, adsorbed water. This required the modification of the free water flux equation (10), whilst the remaining constitutive laws (8)-(16) were unchanged from the Tenchev Model.

Similarly to the work of Gawin et al. [4], the free water is separated into liquid and adsorbed water components, whereby the former is subject to pressure driven flow and the latter diffuses due to a concentration gradient. It is assumed that moisture entering a dry sample of concrete will initially fill the gel pores and adhere to the surface of capillary pores as adsorbed water, up to a maximum

volume, before the remaining capillary pore space fills with liquid water. An analogous process is also assumed to occur in reverse during drying.

The degree of saturation with free water can therefore be described in terms of the free water volume fraction, ε_{FW}, and the porosity, ϕ, as given in (28):

$$S = \frac{\varepsilon_{FW}}{\phi} \tag{28}$$

and the degree of saturation with adsorbed water, S_B, is given by (29):

$$S_B = \begin{cases} S & \text{for } S \le S_{SSP} \\ S_{SSP} & \text{for } S > S_{SSP} \end{cases} \tag{29}$$

where, S_{SSP} is the solid saturation point, i.e. the upper limit of the hygroscopic moisture range and the maximum degree of saturation with adsorbed water [4].

Thus, the free water mass flux equation (10) can be rewritten as (30):

$$\mathbf{J}_{FW} = \underbrace{\left(1 - \frac{S_B}{S}\right)\varepsilon_{FW}\rho_L\mathbf{v}_L}_{\text{Liquid water component}} + \underbrace{\left(\frac{S_B}{S}\right)\varepsilon_{FW}\rho_L\mathbf{v}_B}_{\text{Adsorbed water component}} \tag{30}$$

$\mathbf{v}_B$ being the velocity of the adsorbed water resulting from diffusion (31).

$$\mathbf{v}_B = -D_B\nabla S_B \tag{31}$$

where, D_B is the coefficient of adsorbed water diffusion [4].

$\mathbf{v}_L$ is the velocity of the liquid phase resulting from pressure driven flow as given by Darcy's law (32).

$$\mathbf{v}_L = -\frac{KK_L}{\mu_L}\nabla P_L \tag{32}$$

Equation (32) is identical to equation (12) in the original model, but it is restated here to emphasise that for the Modified Model the liquid pressure is not necessarily equal to the gas pressure, $P_L \neq P_G$. Instead, P_L is calculated from equation (33) below.

$$P_L = P_G - P_C \tag{33}$$

where, P_C is the capillary pressure.

The two new variables the coefficient of adsorbed water diffusion, D_B, and the capillary pressure, P_C, are fundamental to the formulation of the Modified Model. The adsorbed water diffusion coefficient is given by a simple empirical relationship (34) [4]

$$D_B = D_B^0 \exp\left(-2.08\frac{S}{S_{SSP}}\frac{T}{T_{Ref}}\right) \quad \text{for } S \le S_{SSP} \tag{34}$$

and the capillary pressure is calculated via the Kelvin Equation (35).

$$P_C = -R_V T \rho_L \ln\left(\frac{P_V}{P_{Sat}}\right) \tag{35}$$

Where no liquid water exists, i.e. for temperatures above the critical temperature for water and where $S \le S_{SSP}$, capillary pressures are not physically defined and P_C is taken as zero.

In addition to the gas, liquid and capillary pressures, it was also desirable to calculate an average pressure for the fluids present in the concrete pores, to be further employed in a mechanical analysis in order to determine an effective stress, e.g. [4]. The averaged pore pressure, P_{Pore}, was here defined according to (36), assuming that the adsorbed water applies no pressure but in fact behaves as part of the solid skeleton when considering the transfer of stress, and that the effects of the liquid and gas pressures are weighted on a pro rata basis according to their volume fractions in the remaining pore space:

$$P_{Pore} = \begin{cases} P_G - P_{G,\infty} & \text{for } S \le S_{SSP} \\ \left(\frac{S - S_{SSP}}{1 - S_{SSP}}\right)P_L + \left(\frac{1 - S}{1 - S_{SSP}}\right)P_G - P_{G,\infty} & \text{for } S > S_{SSP} \end{cases} \tag{36}$$

where, $P_{G,\infty}$ is the pressure of the atmosphere external to the concrete.

It may be noted that this calculation takes place at the end of the analysis step and has no effect on the behaviour of the transport model. For the purposes of comparison in this paper, equation (36) was implemented as a post-processing feature in both the replication of the Tenchev Model and the Modified Model.

As already stated, in addition to the modifications to the model formulation described above, many of the parameters required for the above formulation are themselves dependent on temperature. A range of different relationships has been suggested by various authors for many of these parameters, e.g. [4, 10, 11], however, in order to maintain as consistent a comparison as possible, these 'auxiliary' relationships used in the Modified Model were unchanged from those used in the Tenchev Model (See Appendix I). The only exceptions to this were the functions describing the relative permeabilities, K_G & K_L.

It has already been stated that the Tenchev Model considered a small, constant value for the relative permeability of the liquid phase, K_L = 0.01, arguing that capillary menisci cause the liquid pressure to be about 100 times lower than the gas pressure (ratio kept constant). The associated relationship for the relative gas permeability was a simple linear function of saturation (37).

$$K_G = 1 - S \tag{37}$$

Given that the Modified Model explicitly considers capillary pressure, it was appropriate to use a more complex, empirical relationship for the relative liquid permeability expressed as a function of the free water saturation. A relationship developed by Van Genuchten and reported by Baroghel-Bouny et al. [12] was chosen (38) and for consistency the associated equation for gas relative permeability was also adopted.

$$K_L = \sqrt{S}\left(1 - \left(1 - S^{1/m}\right)^m\right)^2 \qquad K_G = \sqrt{1-S}\left(1 - S^{1/m}\right)^{2m} \tag{38}$$

where the coefficient m=1/2.2748 [12].

A related sensitivity study showed that the new equation for K_G had little effect on the results since, while the function appears complex, for the chosen value of m it is in fact close to the linear relationship of equation (37).

New material properties for adsorbed water were required for the governing equations (5)-(7) in the Modified Model – the adsorbed water was assumed to behave in a manner equivalent to liquid water, i.e. the density was assumed to remain constant at 1000kg/m^3 and the enthalpy of desorption was assumed to follow the relationship for the enthalpy of evaporation (equation (AI.27)).

As before, the choice of these parametric relationships does not affect the formulation of the differential equations as detailed in the following section.

Numerical Model - Differential Equations

From the conservation equations (5)-(7), it can be seen that altering the mass flux of free water affects both the moisture and energy governing equations. This subsequently affects six terms in the differential equations (19) & (21), namely K_{TT}, K_{TP}, K_{TV}, K_{MT}, K_{MP} and K_{MV}. All other terms remain unchanged. After re-evaluation, the components listed above can be written as follows:

$$K_{TT} = k - \lambda_E \varepsilon_{FW} \rho_L \left(\frac{S_B D_B}{S\phi} \left(\frac{\partial \varepsilon_{FW}}{\partial T} - \frac{\varepsilon_{FW}}{\phi} \frac{\partial \phi}{\partial T} \right) - \left(1 - \frac{S_B}{S} \right) \frac{KK_L R_V \rho_L}{\mu_L} \left(\frac{T}{P_{Sat}} \frac{\partial P_{Sat}}{\partial T} - \left(1 + \frac{T}{\rho_L} \frac{\partial \rho_L}{\partial T} \right) \ln \left(\frac{\tilde{\rho}_V R_V T}{P_{Sat}} \right) - 1 \right) \right) \quad (39)$$

$$K_{TP} = -\lambda_E \left(1 - \frac{S_B}{S} \right) \varepsilon_{FW} \rho_L \frac{KK_L}{\mu_L} \quad (40)$$

$$K_{TV} = -\lambda_E \varepsilon_{FW} \rho_L \left(\left(1 - \frac{S_B}{S} \right) \frac{KK_L}{\mu_L} \frac{R_V T \rho_L}{\tilde{\rho}_V} + \frac{S_B D_B}{S\phi} \frac{\partial \varepsilon_{FW}}{\partial \tilde{\rho}_V} \right) \quad (41)$$

$$K_{MT} = \frac{\varepsilon_G D_{AV} \tilde{\rho}_V P_G}{\tilde{\rho}_G R_A T^2} + \varepsilon_{FW} \rho_L \left(\frac{S_B D_B}{S\phi} \left(\frac{\partial \varepsilon_{FW}}{\partial T} - \frac{\varepsilon_{FW}}{\phi} \frac{\partial \phi}{\partial T} \right) - \left(1 - \frac{S_B}{S} \right) \frac{KK_L R_V \rho_L}{\mu_L} \left(\frac{T}{P_{Sat}} \frac{\partial P_{Sat}}{\partial T} - \left(1 + \frac{T}{\rho_L} \frac{\partial \rho_L}{\partial T} \right) \ln \left(\frac{\tilde{\rho}_V R_V T}{P_{Sat}} \right) - 1 \right) \right) \quad (42)$$

$$K_{MP} = \frac{KK_G}{\mu_G} \varepsilon_G \tilde{\rho}_V - \frac{\varepsilon_G D_{AV} \tilde{\rho}_V}{\tilde{\rho}_G R_A T} + \left(1 - \frac{S_B}{S} \right) \varepsilon_{FW} \rho_L \frac{KK_L}{\mu_L} \quad (43)$$

$$K_{MV} = \frac{\varepsilon_G D_{AV}}{\tilde{\rho}_G} \left(\tilde{\rho}_A + \frac{R_V}{R_A} \tilde{\rho}_V \right) + \varepsilon_{FW} \rho_L \left(\left(1 - \frac{S_B}{S} \right) \frac{KK_L}{\mu_L} \frac{R_V T \rho_L}{\tilde{\rho}_V} + \frac{S_B D_B}{S\phi} \frac{\partial \varepsilon_{FW}}{\partial \tilde{\rho}_V} \right) \quad (44)$$

The overall finite element framework used to solve the Tenchev Model is also used to solve the modified set of differential equations without changes.

2.4. Numerical Model - Boundary Conditions

The treatment of boundary conditions boundary conditions is not affected by the modification of the free water flux equation. The formulation is therefore the same for both the Tenchev Model and the Modified Model.

Equation (45) below represents the energy conservation for the boundary.

$$k \frac{\partial T}{\partial n} - \left(H_G - H_G^0 \right) \mathbf{J}_G \cdot \mathbf{n} + \left(H_G - H_G^0 \right) \beta \left(\tilde{\rho}_G - \tilde{\rho}_{G,\infty} \right) + \lambda_E \mathbf{J}_{FW} \cdot \mathbf{n} + h_{qr} \left(T - T_\infty \right) = 0 \quad (45)$$

where, H_G & $H_G{}^0$ are respectively the enthalpy of the gaseous mixture at current and ambient conditions, β is the coefficient of water vapour mass transfer on the boundary, h_{qr} is the combined

convection and radiation heat transfer coefficient on the boundary, $\tilde{\rho}_{G,\infty}$ & T_∞ are the vapour content and temperature of the atmosphere and **n** is the vector normal to the boundary.

The flux of gaseous material transferred to the boundary from inside the concrete must equal the gaseous material dissipated into the atmosphere from the boundary. Hence, the mass conservation for the gaseous mixture on the boundary can be written as (46):

$$\mathbf{J}_G \cdot \mathbf{n} - \beta\left(\tilde{\rho}_G - \tilde{\rho}_{G,\infty}\right) = 0 \tag{46}$$

It may also be assumed that the surface of the concrete exposed to the atmosphere, especially when exposed to fire, will be dry and consequently there will be no free water (either liquid or adsorbed) flux across the boundary from the concrete to the atmosphere, i.e. $\mathbf{J}_{FW} = 0$.

The energy conservation equation for the boundary (45) may thus be rewritten and rearranged to give the temperature gradient across the boundary as below (47):

$$k\frac{\partial T}{\partial n} + h_{qr}\left(T - T_\infty\right) = 0 \qquad \Rightarrow \frac{\partial T}{\partial n} = \frac{h_{qr}}{k}\left(T_\infty - T\right) \tag{47}$$

For the gas pressure boundary condition, it may be noted that the gas pressure on the boundary will always be equal to the atmospheric pressure and so the gas pressure gradient across the boundary will always be zero (48).

$$\frac{\partial P_G}{\partial n} = 0 \tag{48}$$

Following from the assumption for the mass conservation of gaseous material on the boundary, the mass conservation of water vapour on the boundary can be written as (49):

$$\mathbf{J}_V \cdot \mathbf{n} - \beta\left(\tilde{\rho}_V - \tilde{\rho}_{V,\infty}\right) = 0 \tag{49}$$

From the original derivation of the differential equations by Tenchev et al. [6], it is shown that the water vapour flux can be written as (50):

$$-\mathbf{J}_V = \left(K_{VT}\nabla T + K_{VP}\nabla P_G + K_{VV}\nabla\tilde{\rho}_V\right) \tag{50}$$

Substituting into equation (49) gives:

$$-\left(K_{VT}\nabla T + K_{VP}\nabla P_G + K_{VV}\nabla\tilde{\rho}_V\right)\cdot\mathbf{n} - \beta\left(\tilde{\rho}_V - \tilde{\rho}_{V,\infty}\right) = 0 \tag{51}$$

Therefore:

$$\Rightarrow -\left(K_{VT}\frac{\partial T}{\partial n} + K_{VP}\frac{\partial P_G}{\partial n} + K_{VV}\frac{\partial\tilde{\rho}_V}{\partial n}\right) - \beta\left(\tilde{\rho}_V - \tilde{\rho}_{V,\infty}\right) = 0 \tag{52}$$

Rearranging and substituting in equations (47) and (48) it can be shown that the vapour content gradient across the boundary is:

$$\frac{\partial \tilde{\rho}_V}{\partial n} = -\frac{K_{VT}}{K_{VV}}\frac{h_{qr}}{k}\left(T_\infty - T\right) + \frac{\beta}{K_{VV}}\left(\tilde{\rho}_{V,\infty} - \tilde{\rho}_V\right) \tag{53}$$

Although the boundary conditions are the same for both models it may be noted that in [6] k was replaced with K_{TT} for consistency. In the Modified Model K_{TT} is no longer equal to k and this consistency no longer holds.

2.5. Finite Element Formulation

As shown previously (17)-(21) the governing differential equations can be written in matrix-vector form such that:

$$\mathbf{C}\dot{\mathbf{u}} - \nabla\cdot\left(\mathbf{K}\nabla\mathbf{u}\right) = 0 \tag{54}$$

where,

$$\mathbf{C} = \begin{bmatrix} C_{TT} & C_{TP} & C_{TV} \\ C_{AT} & C_{AP} & C_{AV} \\ C_{MT} & C_{MP} & C_{MV} \end{bmatrix}; \quad \mathbf{K} = \begin{bmatrix} K_{TT} & K_{TP} & K_{TV} \\ K_{AT} & K_{AP} & K_{AV} \\ K_{MT} & K_{MP} & K_{MV} \end{bmatrix}; \quad \mathbf{u} = \begin{pmatrix} T \\ P_G \\ \tilde{\rho}_V \end{pmatrix} \tag{55}$$

By applying Green's Theorem to the weighted residual form of (54), the weak form of the governing equations, expressed for an incremental-iterative solution scheme (at iteration $i + 1$ for a given time step), can be written as (56):

$$\int_V \left[\mathbf{W}\mathbf{C}\dot{\mathbf{u}}^{(i+1)} + \nabla\mathbf{W}\left(\mathbf{K}\nabla\mathbf{u}^{(i+1)}\right)\right]dV - \int_S \mathbf{W}\mathbf{K}\mathbf{q}\; dS = 0 \tag{56}$$

where, $\mathbf{W}$ is a set of arbitrary scalar weighting functions and $\mathbf{u}$ & $\dot{\mathbf{u}}$ are the set of primary variables and their rates, such that:

$$\mathbf{u}^{(i+1)} = \mathbf{u}^i + d\mathbf{u} \qquad \dot{\mathbf{u}}^{(i+1)} = \frac{1}{\Delta t}d\mathbf{u} \tag{57}$$

Discretising in the normal way, (56) & (57) can be rearranged and written in matrix-vector form as:

$$\begin{bmatrix} \mathbf{K_{TT}} & \mathbf{K_{TP}} & \mathbf{K_{TV}} \\ \mathbf{K_{AT}} & \mathbf{K_{AP}} & \mathbf{K_{AV}} \\ \mathbf{K_{MT}} & \mathbf{K_{MP}} & \mathbf{K_{MV}} \end{bmatrix} d\mathbf{a} = \begin{pmatrix} f_{T_{ext}} - f_{T_{\text{int}}} \\ f_{A_{ext}} - f_{A_{\text{int}}} \\ f_{M_{ext}} - f_{M_{\text{int}}} \end{pmatrix} \tag{58}$$

where, for example, the term $\mathbf{K_{TT}}$ is expressed as:

$$\mathbf{K_{TT}} = \int_V \frac{1}{\Delta t}\mathbf{h}^{\mathrm{T}} C_{TT}\mathbf{h} + (\nabla\mathbf{h})^{\mathrm{T}} K_{TT}(\nabla\mathbf{h})\, dV \tag{59}$$

$f_{T_{ext}}$ is expressed as:

$$f_{T_{ext}} = \int_S \mathbf{h}^{\mathrm{T}} K_{TT} \frac{\partial T}{\partial n}\, dS \tag{60}$$

$f_{T_{\mathrm{int}}}$ is expressed as:

$$f_{T_{\mathrm{int}}} = \int_V (\nabla\mathbf{h})^{\mathrm{T}} K_{TT}(\nabla\mathbf{h})\, dV\, \mathbf{a}_T^{(i)} \tag{61}$$

and **h** & **a** are respectively the set of shape functions and the set of discrete primary variables.

3. Numerical Investigation

In order to compare the performance of the two models discussed above and to study the significance of capillary pressure and adsorbed water on the transport of heat and moisture in concrete, the benchmark problem employed by Tenchev et al. [6] was considered. Four analyses with an increasing level of complexity were undertaken. First, the problem was run with the Tenchev Model and then repeated, with the Tenchev Model altered to adopt the relative permeabilities from Baroghel-Bouny [12] (38). A further two analyses were undertaken by introducing different features of the Modified Model, whilst maintaining the permeabilities from Baroghel-Bouny. For the first analysis with the Modified Model, the effect of capillary pressure only was examined. This was done by setting the upper limit of the hygroscopic moisture range, S_{SSP}, to zero, which in turn fixes the degree of saturation with adsorbed water, S_B, to zero at all times. In this case the free water flux equation (30) then reduces to the original equation (10), although the liquid phase velocity is still driven by liquid pressure and the capillary pressure is considered through equation (35). For the second analysis with the Modified Model, the effect of adsorbed water is also accounted for.

Summary of Benchmark Analyses:

- *Analysis 1* - Tenchev Model (reproduction)
- *Analysis 2* – Tenchev Model (relative permeabilites from Baroghel-Bouny (38))
- *Analysis 3* - Modified Model (relative permeabilites (38) and capillary pressure only)
- *Analysis 4* - Modified Model (relative permeabilites (38), capillary pressure and adsorbed water)

Benchmark Problem

The benchmark problem was representative of a section of a concrete column exposed to fire (See *Figure 1*). The model consisted of a rectangular section, 0.2m in length, discretised into 200 elements in the *x*-direction and 1 element in the *y*-direction. Prescribed values of temperature, gas pressure and vapour content were specified for the atmosphere external to the left-hand end of the section. The temperature was defined according to the ISO 834 standard fire curve (62), representative of exposure to an intense fire for a period of 1 hour.

$$T_{\infty} = 20 + 345\log_{10}(8t + 1) + 273.15 \tag{62}$$

where, t is time in minutes, the gas pressure was defined as 0.1MPa, an approximate value for atmospheric pressure and the vapour content was set to 80% of the initial internal vapour content.

In accordance with the boundary conditions discussed previously, the temperature and vapour content were defined as flux boundaries, while the gas pressure was defined as a prescribed boundary. No conditions were defined for the other three boundaries resulting in an effectively 1-dimensional problem.

The initial internal conditions for the concrete were a uniform temperature, T, of 20°C, uniform gas pressure, P_G, equal to 0.1MPa, and a uniform vapour content, $\tilde{\rho}_V$, such that, through the ideal gas law (13), the vapour pressure, P_V, was equal to the saturation pressure of water vapour, P_{Sat}. It may be noted that this defined the initial relative humidity within the concrete pores as 100%. A complete listing of the auxiliary parametric relationships and the material properties employed in the model can be found in Appendix I.

The analyses were conducted using an iterative, mid-point time stepping algorithm. Iterations were limited to 10 but checks on convergence showed that the model rarely exceeded this number and increasing the number of iterations made little difference to the solution. (It may be noted that Tenchev et al. [6] allowed only 5 iterations in their analyses). While the discretisation of the model was the same as that used in the original work, the time step was reduced from 2s to 0.5s.

Numerical Results

As discussed above, the first analysis of the benchmark problem was carried out by reproducing the reproduction of the original Tenchev Model (*Analysis 1*). As can be seen in *Figures 2a - j* the results produced by this model replicate very well the results presented by Tenchev et al. [6] and most of the trends and significant features noted in that work are present in current results as well.

Of particular interest is the appearance of the steep drying front, across which the phase mixture changes from 'high vapour content and low liquid water content' on the hot side to 'low vapour content and high liquid content' on the cold side, and secondly, an increase in water content ahead of the drying front (referred to as the 'moisture clog zone'), where water re-condenses in the cooler zone of the concrete (See *Figures 2i & j*). The reproduced model matches very well with the original Tenchev results both in their magnitudes and in their evolution. A small difference between the liquid water contents (*Figure 2i & j*) is seen in the region between the drying fronts and the 'moisture clog zone', where a clearly defined evaporation zone is present in the results of the original work but is absent from those of *Analysis 1*. Further small differences between the two sets of results can be seen in the temperature profiles (*Figures 2a & b*), where those from *Analysis 1* are slightly less steep than those reported by Tenchev et al. [6], and also, from *Figures 2c -h*, it can be seen that the gas pressure and vapour contents predicted in *Analysis 1* are slightly higher than those reported by Tenchev et al.

These minor differences are thought to be a result a lack of full equivalence between the two simulations.

Mass Conservation Check

Before considering the results of the four *Analyses* in detail a study of the moisture mass conservation is reported, whereby the mass of moisture (i.e. free water and water vapour) lost in the interior of the discretised zone was compared to the total mass of vapour passing through the boundary. It may be noted that the assumed boundary conditions are such that no free water passes through the boundary.

As can be seen in *Figures 3a - d*, that for all cases the mass of vapour lost to the atmosphere matched very well the mass lost in the interior of the concrete. It may also be noted that in all cases oscillations were observed in the internal moisture mass loss. A similar effect was noted by Tenchev et al. [6] and it was considered to be a result of sudden changes in the gradient of the Sorption Isotherms that result in instantaneous imbalances in the moisture mass conservation that are however rebalanced over time. A further contribution to this effect may be the difficulty in capturing the almost vertical nature of the drying front within a discretised region. The drying front jumps from one element to another as it recedes, causing discretisation errors in the mass balance as it does so. Again, this effect will rebalance over time.

Comparison of Results from *Analysis 1, 2, 3 & 4*

Again as discussed, three further analyses of the benchmark problem were carried out, first with the Tenchev Model formulation altered by adopting the relative permeabilities from Baroghel-Bouny [12] (equation (38)) (*Analysis 2*), and secondly, with the Modified Model, considering either capillary pressure only (*Analysis 3*) or considering both capillary pressure and adsorbed water (*Analysis 4*). *Analysis 3* is included in order to isolate the effect of adsorbed water while *Analysis 4* is believed to be the most realistic. Comparative plots showing the results of *Analyses 1*, *2*, *3* & *4* after 1 hour of exposure to fire are shown in *Figures 4a - j*.

As can be seen in *Figure 4a*, the temperature profiles from all four analyses are virtually identical, indicating that the differences in fluid transport predicted by the two models have little effect on the heat transfer. This is indeed expected since the convection term, $\underline{(\rho C \mathbf{v})} \cdot \nabla T$ in the governing equation (7), is ignored in both models (See Part 1 above).

It can also be seen in *Figure 4* that the main features discussed above in reference to the original work [6], e.g. the steep drying fronts and peaks in gas pressure and vapour content, are also clearly visible in both sets of results from the Modified Model. It may further be noted that the rates of evolution of the profiles for all three analyses are very similar. However, significant differences are noted for the results pertaining to gas and liquid pressures and vapour and liquid contents (*Figures*

4b - j), although it is also clear that the results of *Analysis 2* are extremely similar to those of *Analysis 3*. The significance of this will be discussed in due course.

As can be seen in *Figures 4b & c*, the peaks of the gas pressure and vapour content profiles predicted in *Analyses 2, 3 & 4* are more diffuse than their respective counterparts from *Analysis 1* and that their maxima occur at the drying fronts rather than ahead of them (c.f. *Figure 4g*). It may also be seen that the maximum values predicted are lower than those from *Analysis 1*, by approximately 20-25% for *Analyses 2 & 3* and by 10-15% for *Analysis 4*.

The lower predicted gas pressures obviously affect the averaged pore pressures (*Figure 4h*) calculated according to equation (36) and this in turn has significance when considering the potential for spalling, a principal cause of which is thought be the internal pore pressure of the concrete.

The lower predicted vapour contents have several effects on the overall behaviour of the model. Firstly, they are partly responsible for the described differences in the gas pressure profiles since vapour content and gas pressure are directly linked via the ideal gas law (13) and Dalton's law (14). Secondly, since the vapour content controls the relative humidity, it is also directly associated with the free water content, via the ideal gas law (13) and the Sorption Isotherms (15), and the differences in the predicted vapour contents must therefore be related to the differences that can be seen in the water content profiles for the three sets of results (*Figure 4g*).

From *Figure 4g* it can be seen that the results from *Analyses 2, 3 & 4* show larger areas of increased water content ahead of the drying front, and thus more extensive 'moisture clog zones', than the results of *Analysis 1*. This observation is consistent with the profiles in *Figure 4c*, which show that significantly higher vapour contents are predicted in this region in *Analyses 2, 3 & 4*, leading directly to the higher liquid content via the Sorption Isotherms. The physical mechanism behind this can be explained by *Figure 4j*, where it can be seen that in *Analysis 1*, the original formulation of the Tenchev Model predicts a much higher water vapour flux towards the face exposed to fire than is predicted in any of the other three *Analyses* and consequently there is less vapour ahead of the drying front available to condense into liquid water.

In addition to this effect, the liquid water is more easily able to flow away into the cooler regions of the concrete due to the increased fluid transport capacity predicted by both the altered

Tenchev Model (*Analysis 2*) and the Modified Model (*Analyses 3 & 4*). This accounts for the more extensive 'moisture clog zones' and comes about through two processes. Firstly, for *Analyses 2,3* and *4*, the relative permeability of the liquid phase, K_L, is not fixed as in *Analysis 1* and is generally much higher since it is related to the saturation according to equation (38) and ranges between 0.0 and 1.0. Secondly, for *Analyses 3 & 4*, the free water flux equation (30) is formulated in terms of the liquid pressure, P_L, rather than the gas pressure, P_G, (as in *Analysis 1*) and is directly affected by the inclusion of the capillary pressure terms (See Appendix II).

However, since the results of *Analysis 2*, in which the new relationship for K_L is used while the rest of the Tenchev Model remains unchanged, are almost identical to those of *Analysis 3*, in which the Modified Model is employed and both the new relationship for K_L and explicit consideration of capillary pressure are employed, it is clear that the change in K_L has by far the greatest effect on the transport behaviour under the conditions applied in the benchmark problem.

As can be seen in *Figure 4f*, due to the increased fluid transport, the liquid pressure profiles predicted in *Analyses 2*, *3* & *4* are less steep and consequently of a greater extent than those of *Analysis 1*. This results in a much larger region of concrete in which the liquid pressure gradient drives liquid water away from the face exposed to fire and into the cooler regions of the concrete. Furthermore, while the peaks of the liquid pressure profiles predicted in *Analyses 2*, *3* & *4* occur at the drying front (coincident with the gas pressure profiles discussed previously), the peak in *Analysis 1* occurs ahead of the drying front and consequently there is a small region in which the pressure gradient drives liquid water towards the face exposed to fire and evaporation (hence the larger flux of vapour towards the boundary).

These observations are confirmed by the plot of the free water fluxes (*Figure 4i*), which illustrates the generally higher free water transport predicted in *Analyses 2*, *3* & *4*. However, from *Figures 4g & i*, it may also be seen that the increase in transport capacity gained through the modification of the free water flux equation is partially lost when adsorbed water is considered and only the liquid fraction of the free water is driven by the liquid pressure gradient. This can be explained by considering the regions ahead and behind the drying front. In the region ahead of the drying front, where the largest free water fluxes are seen, liquid water is present and adsorbed water

saturation, S_B, is at its maximum value, equal to S_{SSP}, there is no gradient of S_B and the adsorbed water does not flow. Thus it can be seen that the free water flux from *Analysis 4*, consisting of only the liquid water flowing under a pressure gradient, is lower than those of *Analyses 2 & 3* (*Figure 4i*) in which all free water is considered to flow under a pressure gradient and the difference between the profiles is the effect of considering adsorbed water behaviour as distinct from liquid water behaviour. Furthermore, in the region behind the drying front, where free water content is very low or zero, there is almost no free water flux (liquid or adsorbed) predicted by any of the *Analyses*. As such there is almost no adsorbed water flux predicted anywhere in the concrete during *Analysis 4*.

Therefore, although Tenchev's assumption that adsorbed flux is negligible and can consequently be ignored is, at first glance, reasonable, *Figure 4i* illustrates that recognising the large fraction of free water held in the wet region as adsorbed water is extremely important and that to ignore it and thus assume that all free water can be convected under pressure driven flow can have a significant effect not only on the free water flux but also on the vapour content and gas pressures (*Figures 4b - j*).

Capillary Pressure in *Analyses 1, 2, 3 & 4*

The most significant difference between the results of the four *Analyses* is the difference in the predicted liquid pressures and which potentially has significant implications for the fluid transport behaviour. In the Tenchev Model (*Analyses 1 & 2*), the liquid pressure is assumed to be equal to the gas pressure and therefore the capillary pressure (defined as $P_C = P_G - P_L$) is apparently always zero (*Figure 4d*). In the Modified Model, since capillary pressure is explicitly considered, the liquid and gas pressures are not necessarily equal (*Figure 4b & f*). As can be deduced from the Kelvin Equation (35) the capillary pressure increases rapidly with the reduction in relative humidity. Therefore, in the drying zone just behind the drying front, where the temperature is below the critical value and free water is present, high capillary pressures may be expected. This can be clearly seen in the results from *Analysis 3* in *Figure 4d*, where capillary pressures of more than 400MPa were predicted, resulting in similarly large negative liquid pressures in the same region (*Figure 4f*). No capillary

pressures were predicted ahead of the drying zone where the relative humidity did not drop below the initial value of 100% and the liquid and gas pressures were indeed equal.

It is interesting to note that, irrespective of the capillary pressures predicted in *Analysis 3*, the overall results are very similar to those of *Analysis 2*, with only a small difference in the peak pore pressures (*Figure 4h*). This suggests that the capillary pressures have little or no effect on the transport behaviour in concrete under intense heating (largely because they only exist in a region where there is almost no water content), which in turn supports the approximation of $P_G = P_L$ for the problem of concrete exposed to fire, as adopted in the Tenchev Model [6] for the problem of concrete exposed to fire. Furthermore, it questions the need to account for the influence of capillary pressure at all, as was the case with the Tenchev Model via an artificially reduced relative permeability for liquid.

The insignificance of capillary pressures in problems of concrete exposed to fire appears to be further borne out by the results of *Analysis 4*, which despite explicitly considering capillary pressure, did not predict any. This effect is again due to the consideration of adsorbed water and also associated with the steep nature of the drying front. Behind the drying front, the water content drops very rapidly below the solid saturation point, S_{SSP}. Below this point, there is no liquid water, only adsorbed water is present, and so, although the relative humidity is less than 100%, capillary menisci cannot develop.

It can furthermore be argued that, by considering the physical behaviour of adsorbed water as distinct from the that of liquid water, the results of *Analysis 4* are more representative of the physical behaviour of a hygroscopic material such as a concrete than those of *Analysis 3*, since below approximately 50% relative humidity capillary menisci become unstable and dissipate, leaving only a film of adsorbed water on the surface of the solid [13, 14]. Consequently, from the Kelvin Equation (35), capillary pressures in the range ~100-200MPa represent the maximum achievable level. The capillary pressures predicted in *Analysis 3*, when adsorbed water behaviour is neglected, are unrealistically high.

4. Conclusions

The Modified Model was presented as a modification and extension of the Tenchev Model to include explicitly capillary pressure and adsorbed water behaviour in the finite element analysis of heat and moisture transfer in concrete exposed to fire. Studies were carried out to investigate the effect of these modifications and to assess the significance of related modelling assumptions and approximations made in the Tenchev Model.

When applied to the problem of concrete exposed to intense heating, the original formulation of the Tenchev Model, with the relative permeability for liquid water artificially restricted in order to represent the influence of capillary pressure, was found to under predict the fluid transport capacity in the concrete and consequently over predict the gas pressure and vapour content (by up to 25%) in comparison with the altered model when the relative permeability was allowed to vary with the degree of saturation. This shows that the original formulation of the Tenchev Model would be conservative when utilised in the prediction of mechanical damage phenomena, such as spalling, which are related to pore pressures.

It was furthermore found that the Modified Model, with only capillary pressure explicitly considered, produced very similar results to the original Tenchev Model, thereby indicating that capillary pressure is relatively unimportant in the heat and moisture transport behaviour in concrete exposed to fire, which provides numerical evidence in support of the previously unsupported assumptions made by Tenchev et al.

When the Modified Model considering both capillary pressure and adsorbed water behaviour was applied to the same problem, no capillary pressures were predicted, again emphasising that the inclusion of capillary pressure may be unnecessary. However, the gas pressures and vapour contents predicted were higher than those seen for the altered Tenchev Model and the Modified Model including capillary pressures only. As with the original Tenchev Model, this was caused by a reduction in the predicted fluid transport capacity due to the diffusion rather than pressure driven flow of adsorbed water. Although more work is required to study the flux behaviour of adsorbed water in these conditions, the constitutive laws employed in the Modified Model are based on clear physical concepts and it is felt that the flow behaviour predicted is quite representative. It was also noted that

the inclusion of adsorbed water behaviour allowed the model to naturally capture realistic capillary pressure behaviour, whereas without adsorbed water the Modified Model predicted non-physical capillary pressures,

In summary, it has been shown that capillary pressures have little effect on the fluid transport behaviour in concrete exposed to high temperatures and whether they are ignored or explicitly included in a model formulation appears to make little difference. However, it may also be noted that in order to make the model generally applicable to problems of heating or even drying of concrete (i.e. not only high temperature), where significant capillary pressures may develop, it should be included in the model formulation.

It has also been shown that although the actual flux of adsorbed water is minimal in problems of concrete exposed to high temperature, the consideration of its behaviour can nevertheless have a significant effect on the fluid transport behaviour and the predicted vapour content and the gas pressures. Ignoring this behaviour may lead to under prediction of the pore pressures in concrete and to an overestimation of its resistance to mechanical damage such as spalling.

Acknowledgements

This work was carried out as part of the MAECENAS research project "Modelling of ageing in concrete nuclear power plants", supported by the European Community through the EURATOM programme (Contract no. FIKS-CT-2001-00186).

References

1. Ulm, F.-J., Coussy, O. and Bažant, Z. P., The "Chunnel" Fire. I: Chemoplastic Softening in Rapidly Heated Concrete, *Journal of Engineering Mechanics*, 1999; **125**(3): p. 272 - 282.
2. Neville, A.M., *Properties of Concrete*. 2nd ed, 1973: Pitman.
3. Coussy, O., *Mechanics of Porous Continua*, 1995; Chichester: Wiley & Sons.
4. Gawin, D., Majorana, C. E. & Schrefler, B. A., Numerical Analysis of Hygro-Thermal Behaviour and Damage of Concrete at High Temperature, *Mechanics of Cohesive-Frictional Materials*, 1999; **4**: p. 37 - 74.

5. Lewis, R.W., & Schrefler, B. A., *The Finite Element Method in the Static and Dynamic Deformation and Consolidation of Porous Media*. 2nd ed, 1998: Wiley.

6. Tenchev, R.T., Li, L. Y. & Purkiss, J. A., Finite Element Analysis of Coupled Heat and Moisture Transfer in Concrete Subjected to Fire, *Numerical Heat Transfer, Part A*, 2001; **39**: p. 685 - 710.

7. Bažant, Z.P., Hauggaard, A. B., Baweja, S. & Ulm, F-J., Microprestress-Solidification Theory for Concrete Creep, I: Aging and Drying Effects, *Journal of Engineering Mechanics*, 1997; **123**(11): p. 1188 - 1194.

8. Cengel, Y.A., *Heat Transfer: A Practical Approach*. 2nd ed, 2003; New York: McGraw-Hill.

9. Bažant, Z.P., & Kaplan, M. F., *Concrete at High Temperatures: Material Properties and Mathematical Models*, 1996; Harlow: Longman.

10. *EN 1992-1-2, Eurocode 2: Design of Concrete Structures*, 1992.

11. Ichikawa, Y., Prediction of Pore Pressures, Heat and Moisture Transfer Leading to Spalling of Concrete During Fire, 2000; Ph.D Thesis, Imperial College: London.

12. Baroghel-Bouny, V., Mainguy, M. Lassabatere, T. & Coussy, O., Characterization and Identification of Equilibrium and Transfer Moisture Properties for Ordinary and High-Performance Cementitious Materials, *Cement and Concrete Research*, 1999; **29**: p. 1225 - 1238.

13. Grasley, Z.C., David A. Lange, D. A. & D'Ambrosia, M. D., New Embedded Sensor for Measuring Relative Humidity of Concrete, *submitted to Cement and Concrete Research*, 2002.

14. Pesavento, F., Nonlinear Modelling of Concrete as Multiphase Porous Material in High Temperature Conditions, in *Department of Construction and Transportation*, 2000; PhD Thesis, University of Padova.

Appendix I – Parametric Relationships

Explanations are given where these relationships differ from those employed by Tenchev et al. [6],

Cement content per unit volume concrete:

$$\text{Constant value, } \varepsilon_{Cem}\rho_{Cem} = 300\text{kg/m}^3 \tag{AI.1}$$

Coefficient of Adsorbed Water Diffusion [4]:

$$D_B = D_B^0 \exp\left(-2.08\frac{S}{S_{SSP}}\frac{T}{T_{Ref}}\right) \quad \text{for } S \le S_{SSP} \tag{AI.2}$$

where, $D_B{}^0 = 1.57 \times 10^{-11}$ m^2/s, $T_{Ref} = 295.0$°K and S_{SSP} is the solid saturation point (See AI.25)

Coefficient of Water Vapour Mass Transfer:

$$\beta = \frac{h_q}{(\rho C)_{Air}}\left(\frac{D_{AV}(T_\infty)}{\alpha_{Air}}\right)^{2/3} \tag{AI.3}$$

where, h_q is the convective heat transfer coefficient and $(\rho C)_{Air}$ & α_{Air} are respectively the heat capacity and thermal diffusivity of air.

Coefficients of Water Vapour/Air Diffusion within porous concrete:

$$D_{AV} = D_{VA} = D\frac{\delta}{\tau^2} \tag{AI.4}$$

$$D = 1.87\times10^{-5}\left(\frac{T^{2.072}}{P_G}\right) \tag{AI.5}$$

where, D is the atmospheric diffusion coefficient of air in water vapour (or water vapour in air), and δ (=0.5) & τ (= 3) are respectively is the constrictivity and tortuosity factors of the concrete, which represent the reduction in the rate of diffusion caused by the complex pore structure of the concrete.

Density of Liquid Water:

$$\text{Constant value, } \rho_L = 1000\text{kg/m}^3 \tag{AI.6}$$

Density of Solid Skeleton:

$$\text{Constant value, } \rho_S = 2400\text{kg/m}^3 \tag{AI.7}$$

Dynamic Viscosities:

Liquid Water: $$\mu_L = 0.6612(T-229)^{-1.562} \text{ for } T \le T_{Crit} \quad \text{(AI.8)}$$

where, T_{Crit} = 647.3°K is the critical temperature for water. Equation (AI.8) was reported by Gawin et al. [4] and fits very well the tabulated data referenced by Tenchev et al. [6].

Water Vapour: $$\mu_V = \mu_V^0 + \alpha_V (T - T_0) \quad \text{(AI.9)}$$

where, $\mu_V{}^0$ = 8.85 × 10^{-6} Pa.s, α_V = 3.53 × 10^{-8} Pa.s.°K^{-1} and T_0 = 273.15°K

Dry Air: $$\mu_A = \mu_A^0 + \alpha_A (T - T_0) - \beta_A (T - T_0)^2 \quad \text{(AI.10)}$$

where, $\mu_A{}^0$ = 17.17 × 10^{-6} Pa.s, α_A = 4.73 × 10^{-8} Pa.s.°K^{-1} and β_A = 2.22 × 10^{-11} Pa.s.°K^{-2}. Equations (AI.9) & (AI.10) were also reported by Gawin et al. [4] and fit well the tabulated data referenced by Tenchev et al. [6] particularly in the temperature range up to ~600°K.

Gaseous Mixture: $$\mu_G = \begin{cases} \dfrac{\tilde{\rho}_A \mu_A + \tilde{\rho}_V \mu_V}{\tilde{\rho}_A + \tilde{\rho}_V} & \text{for } (\tilde{\rho}_A + \tilde{\rho}_V) > 0.0 \\ 0.0 & \text{for } (\tilde{\rho}_A + \tilde{\rho}_V) = 0.0 \end{cases} \quad \text{(AI.11)}$$

Effective Heat Capacity of Concrete: $$\underline{\rho C} = \varepsilon_S \rho_S C_S + \varepsilon_{FW} \rho_L C_{FW} + \varepsilon_G \tilde{\rho}_V C_V + \varepsilon_G \tilde{\rho}_A C_A \quad \text{(AI.12)}$$

where, $\varepsilon_S \rho_S$ is the solid skeleton content per unit volume of concrete and C_i is the specific heat of the phase i.

Emissivity of concrete surface: Constant value, e = 0.6 (AI.13)

Gas Constants:

Air: Constant value, R_A = 287J/kg.°K (AI.14)

Water Vapour: Constant value, R_V = 461.5J/kg.°K (AI.15)

Heat Transfer Coefficients:

Convective: Constant value, $h_q = 25\text{W/m}^2\text{.°K}$ (AI.16)

Radiative:
$$h_r = e\sigma\left(T^2 + T_\infty^2\right)\left(T + T_\infty\right) \quad \text{(AI.17)}$$

where, e is the emissivity of the concrete surface (See AI.13) and σ is the Stefan-Boltzman constant (See AI.32).

Combined:
$$h_{qr} = h_q + h_r \quad \text{(AI.18)}$$

Intrinsic Permeability of Concrete:
$$K = K^0\left(\frac{\phi}{\phi^0}\right)^{2/3} \quad \text{(AI.19)}$$

where, the initial permeability, $K^0 = 5.0 \times 10^{-17}\text{m}^2$ and the initial porosity, $\phi^0 = 0.08$.

Mass of Dehydrated Water:
$$\varepsilon_D \rho_L = \varepsilon_{Cem}\rho_{Cem} \times \begin{cases} 0 & \text{for } \left(T_C \le 200°\text{C}\right) \\ 7.0\times10^{-4}\left(T_C - 200\right) & \text{for } \left(200°\text{C} < T_C \le 300°\text{C}\right) \\ 0.4\times10^{-4}\left(T_C - 200\right) + 0.07 & \text{for } \left(300°\text{C} < T_C \le 800°\text{C}\right) \\ 0.09 & \text{for } \left(T_C > 300°\text{C}\right) \end{cases} \quad \text{(AI.20)}$$

where, T_C is the temperature in °C.

Porosity:
$$\phi = \phi^0 \times \begin{cases} 1 & \text{for } \left(T_C < 100°\text{C}\right) \\ aT_C^3 + bT_C^2 + cT_C + d & \text{for } \left(100°\text{C} \le T_C \le 800°\text{C}\right) \\ 3 & \text{for } \left(T_C > 800°\text{C}\right) \end{cases} \quad \text{(AI.21)}$$

where, the initial porosity, $\phi^0 = 0.08$ and a, b, c & d are coefficients of a cubic function such that $\phi(T)$ and its derivative, $\frac{d\phi}{dT}$, are continuous.

Thermal Conductivity of Concrete:
$$k = 2.0 - 0.24\left(\frac{T_C}{120}\right) - 0.012\left(\frac{T_C}{120}\right)^2 \quad \text{(AI.22)}$$

Saturation Vapour Pressure: $P_{Sat} = aT^6 + bT^5 + cT^4 + dT^3 + eT^2 + fT + g$ for $T \le T_{Crit}$ (AI.23)

where, a = -1.43742221944687 × 10^{-9}, b = 4.42439058302123 × 10^{-6}, c = -3.92808082125791 × 10^{-3}, d = 1.59103252944303, e = -3.25887438504847 × 10^{2}, f = 3.21477952751975 × 10^{4} and g = -1.15466360325087 × 10^{6}. Equation (AI.23) was developed by curve fitting to the tabulated data referenced by Tenchev et al. [6].

Saturation Free Water Content: Constant value, $\varepsilon_{FW}{}^{0}\rho_{L}{}^{0}$ = 60kg/m^3 (AI.24)

Solid Saturation Point: Constant value, $S_{SSP} = 0.55$ when adsorbed water considered
Or, $S_{SSP} = 0.0$ when adsorbed water ignored (AI.25)

Values deduced from the work of Gawin et al. [4].

Specific Enthalpies:

Dehydration of Chemically Bound Water: Constant value, λ_D = 2400 × 10^3J/kg (AI.26)

Evaporation (and desorption): $$\lambda_E = 2.672\times10^5\left(T_{Crit}-T\right)^{0.38} \quad \text{(AI.27)}$$

Equation (AI.27) was reported by Gawin et al. [4] and fits very well the tabulated data referenced by Tenchev et al. [6]. It is also assumed to be valid for desorption of physically bound water.

Specific Heats:

Dry Air: $$C_A = aT^3 + bT^2 + cT + d \quad \text{(AI.28)}$$

where, a = -9.84936701814735 × 10^{-8}, b = 3.56436257769861 × 10^{-4}, c = -1.21617923987757 × 10^{-1} and d = 1.01250255216324 × 10^{3}. Equation (AI.28) was developed by curve fitting to the tabulated data referenced by Tenchev et al. [6].

Free Water: $$C_{FW} = \begin{cases} \left(2.4768T + 3368.2\right) + \left(\dfrac{aT}{513.15}\right)^b & \text{for } T \le T_{Crit} \\ 24515.0 & \text{for } T > T_{Crit} \end{cases} \quad \text{(AI.29)}$$

where, a = 1.08542631988638 and b = 31.4447657616636. Equation (AI.29) was developed by curve fitting to the tabulated data referenced by Tenchev et al. [6].

Solid Skeleton:

$$C_S = 900 + 80\left(\frac{T_C}{120}\right) - 4\left(\frac{T_C}{120}\right)^2 \tag{AI.30}$$

Water Vapour:

$$C_V = \begin{cases} (7.1399T - 443) + \left(\dfrac{aT}{513.15}\right)^b & \text{for } T \le T_{Crit} \\ 45821.04 & \text{for } T > T_{Crit} \end{cases} \tag{AI.31}$$

where, a = 1.13771502228162 and b = 29.4435287521143. Equation (AI.31) was developed by curve fitting to the tabulated data referenced by Tenchev et al. [6].

Stefan-Boltzman constant: Constant value, $\sigma = 5.67 \times 10^{-8} \text{W/m}^2.^\circ\text{K}^4$ (AI.32)

Volume Fraction of Free Water: Sorption Isotherms

$$\varepsilon_{FW} = \begin{cases} \left(\dfrac{\varepsilon_{Cem}\rho_{Cem}}{\rho_L}\right)\left(\dfrac{\varepsilon^0_{FW}\rho^0_L}{\varepsilon_{Cem}\rho_{Cem}}\dfrac{P_V}{P_{Sat}}\right)^{1/m} & \text{for } \left(\dfrac{P_V}{P_{Sat}}\right) \le 0.96 \\ a\left(\dfrac{P_V}{P_{Sat}}\right)^3 + b\left(\dfrac{P_V}{P_{Sat}}\right)^2 + c\left(\dfrac{P_V}{P_{Sat}}\right) + d & \text{for } 0.96 < \left(\dfrac{P_V}{P_{Sat}}\right) < 1.04 \\ \dfrac{\varepsilon^0_{FW}\rho^0_L}{\rho_L}\left(1 + 0.12\left(\dfrac{P_V}{P_{Sat}} + 1.04\right)\right) & \text{for } \left(\dfrac{P_V}{P_{Sat}}\right) \ge 1.04 \end{cases} \tag{AI.33}$$

where, a, b, c & d are complex temperature dependent coefficients of a cubic function such that ε_{FW} and its derivatives $\frac{\partial \varepsilon_{FW}}{\partial (P_V/P_{Sat})}$, $\frac{\partial \varepsilon_{FW}}{\partial T}$ & $\frac{\partial \varepsilon_{FW}}{\partial \tilde{p}_V}$ are always continuous, and m is a temperature dependent coefficient as given by (AI.34):

$$m = 1.04 - \frac{(T_C + 10)^2}{(T_C + 10)^2 + 22.3(25 + 10)^2} \tag{AI.34}$$

The cubic function fitted to the intermediate section of the sorption curves, $0.96 < P_V/P_{Sat} < 1.04$, was developed in order to reproduce the 'smoothed transition' described but not defined by Tenchev et al. [6]. The complex coefficients were themselves functions of temperature and specific to the other parameters of the sorption curves.

Appendix II – derivation of free water flux

$$-J_{FW}=\left(1-\frac{S_B}{S}\right)\varepsilon_{FW}\rho_L\frac{KK_L}{\mu_L}\nabla P_L+\left(\frac{S_B}{S}\right)\varepsilon_{FW}\rho_L D_B\nabla S_B \tag{AII.1}$$

$$P_L=P_G-P_C \tag{AII.2}$$

$$\Rightarrow -J_{FW}=\left(1-\frac{S_B}{S}\right)\varepsilon_{FW}\rho_L\frac{KK_L}{\mu_L}\nabla\left(P_G-P_C\right)+\left(\frac{S_B}{S}\right)\varepsilon_{FW}\rho_L D_B\nabla S_B \tag{AII.3}$$

$$\nabla\left(P_G-P_C\right)=\nabla P_G-\frac{\partial P_C}{\partial T}\nabla T-\frac{\partial P_C}{\partial\tilde{\rho}_V}\nabla\tilde{\rho}_V \tag{AII.4}$$

$$P_C=-R_V T\rho_L\ln\left(\frac{P_V}{P_{Sat}}\right) \tag{AII.5}$$

$$P_V=R_V\tilde{\rho}_V T \tag{AII.6}$$

$$\Rightarrow P_C=-R_V T\rho_L\ln\left(\frac{R_V\tilde{\rho}_V T}{P_{Sat}}\right) \tag{AII.7}$$

$$\frac{\partial P_C}{\partial T}=R_V\rho_L\left(\frac{T}{P_{Sat}}\frac{\partial P_{Sat}}{\partial T}-\left(1+\frac{T}{\rho_L}\frac{\partial\rho_L}{\partial T}\right)\ln\left(\frac{\tilde{\rho}_V R_V T}{P_{Sat}}\right)-1\right) \tag{AII.8}$$

$$\frac{\partial P_C}{\partial\tilde{\rho}_V}=-\frac{R_V T\rho_L}{\tilde{\rho}_V} \tag{AII.9}$$

$$\Rightarrow\nabla\left(P_G-P_C\right)=\nabla P_G-\left(R_V\rho_L\left(\frac{T}{P_{Sat}}\frac{\partial P_{Sat}}{\partial T}-\left(1+\frac{T}{\rho_L}\frac{\partial\rho_L}{\partial T}\right)\ln\left(\frac{\tilde{\rho}_V R_V T}{P_{Sat}}\right)-1\right)\right)\nabla T+\left(\frac{R_V T\rho_L}{\tilde{\rho}_V}\right)\nabla\tilde{\rho}_V \tag{AII.10}$$

$$S_B=\begin{cases}S=\dfrac{\varepsilon_{FW}}{\phi} & \text{for } S\le S_{SSP}\\ S_{SSP}=Const & \text{for } S>S_{SSP}\end{cases} \tag{AII.11}$$

$$\Rightarrow\nabla S_B=\begin{cases}\nabla S=\nabla\left(\dfrac{\varepsilon_{FW}}{\phi}\right) & \text{for } S\le S_{SSP}\\ \nabla S_{SSP}=0 & \text{for } S>S_{SSP}\end{cases} \tag{AII.12}$$

$$\Rightarrow\nabla S_B=\frac{\phi\nabla\varepsilon_{FW}-\varepsilon_{FW}\nabla\phi}{\phi^2}\ \text{for } S\le S_{SSP} \tag{AII.13}$$

$$\varepsilon_{FW}=\varepsilon_{FW}\left(P_V\left(\tilde{\rho}_V,T\right),P_{Sat}(T),\rho_L(T),m(T)\right) \tag{AII.14}$$

$$\nabla\varepsilon_{FW}=\frac{\partial\varepsilon_{FW}}{\partial\tilde{\rho}_V}\nabla\tilde{\rho}_V+\frac{\partial\varepsilon_{FW}}{\partial T}\nabla T \tag{AII.15}$$

$$\phi=\phi(T) \tag{AII.16}$$

$$\nabla\phi = \frac{\partial\phi}{\partial T}\nabla T \tag{AII.17}$$

$$\Rightarrow \nabla S_B = \frac{\phi\left(\frac{\partial\varepsilon_{FW}}{\partial\tilde{\rho}_V}\nabla\tilde{\rho}_V + \frac{\partial\varepsilon_{FW}}{\partial T}\nabla T\right) - \varepsilon_{FW}\left(\frac{\partial\phi}{\partial T}\nabla T\right)}{\phi^2} \tag{AII.18}$$

$$= \frac{1}{\phi}\left(\frac{\partial\varepsilon_{FW}}{\partial T} - \frac{\varepsilon_{FW}}{\phi}\frac{\partial\phi}{\partial T}\right)\nabla T + \frac{1}{\phi}\frac{\partial\varepsilon_{FW}}{\partial\tilde{\rho}_V}\nabla\tilde{\rho}_V \tag{AII.19}$$

$$\Rightarrow -J_{FW} = \left(1-\frac{S_B}{S}\right)\varepsilon_{FW}\rho_L\frac{KK_L}{\mu_L}\nabla\left(P_G - P_C\right) + \left(\frac{S_B}{S}\right)\varepsilon_{FW}\rho_L D_B\nabla S_B \tag{AII.20}$$

$$-J_{FW} = \left(1-\frac{S_B}{S}\right)\varepsilon_{FW}\rho_L\frac{KK_L}{\mu_L}\left(\nabla P_G - \left(R_V\rho_L\left(\frac{T}{P_{Sat}}\frac{\partial P_{Sat}}{\partial T} - \left(1+\frac{T}{\rho_L}\frac{\partial\rho_L}{\partial T}\right)\ln\left(\frac{\tilde{\rho}_V R_V T}{P_{Sat}}\right) - 1\right)\right)\nabla T + \left(\frac{R_V T\rho_L}{\tilde{\rho}_V}\right)\nabla\tilde{\rho}_V\right)$$
$$+\left(\frac{S_B}{S}\right)\varepsilon_{FW}\rho_L D_B\left(\frac{1}{\phi}\frac{\partial\varepsilon_{FW}}{\partial\tilde{\rho}_V}\nabla\tilde{\rho}_V + \frac{1}{\phi}\left(\frac{\partial\varepsilon_{FW}}{\partial T} - \frac{\varepsilon_{FW}}{\phi}\frac{\partial\phi}{\partial T}\right)\nabla T\right) \tag{AII.21}$$

$$= \varepsilon_{FW}\rho_L\left(\frac{S_B D_B}{S\phi}\left(\frac{\partial\varepsilon_{FW}}{\partial T} - \frac{\varepsilon_{FW}}{\phi}\frac{\partial\phi}{\partial T}\right) - \left(1-\frac{S_B}{S}\right)\frac{KK_L R_V\rho_L}{\mu_L}\left(\frac{T}{P_{Sat}}\frac{\partial P_{Sat}}{\partial T} - \left(1+\frac{T}{\rho_L}\frac{\partial\rho_L}{\partial T}\right)\ln\left(\frac{\tilde{\rho}_V R_V T}{P_{Sat}}\right) - 1\right)\right)\nabla T$$
$$+\left(1-\frac{S_B}{S}\right)\varepsilon_{FW}\rho_L\frac{KK_L}{\mu_L}\nabla P_G$$
$$+\varepsilon_{FW}\rho_L\left(\left(1-\frac{S_B}{S}\right)\frac{KK_L}{\mu_L}\frac{R_V T\rho_L}{\tilde{\rho}_V} + \frac{S_B D_B}{S\phi}\frac{\partial\varepsilon_{FW}}{\partial\tilde{\rho}_V}\right)\nabla\tilde{\rho}_V \tag{AII.22}$$

$$\Rightarrow -J_{FW} = K_{LT}\nabla T + K_{LP}\nabla P_G + K_{LV}\nabla\tilde{\rho}_V \tag{AII.23}$$

For $S \le S_{SSP}$

$$K_{LT} = \varepsilon_{FW}\rho_L\left(\frac{S_B D_B}{S\phi}\left(\frac{\partial\varepsilon_{FW}}{\partial T} - \frac{\varepsilon_{FW}}{\phi}\frac{\partial\phi}{\partial T}\right) - \left(1-\frac{S_B}{S}\right)\frac{KK_L R_V\rho_L}{\mu_L}\left(\frac{T}{P_{Sat}}\frac{\partial P_{Sat}}{\partial T} - \left(1+\frac{T}{\rho_L}\frac{\partial\rho_L}{\partial T}\right)\ln\left(\frac{\tilde{\rho}_V R_V T}{P_{Sat}}\right) - 1\right)\right) \tag{AII.24}$$

$$K_{LP} = \left(1-\frac{S_B}{S}\right)\varepsilon_{FW}\rho_L\frac{KK_L}{\mu_L} \tag{AII.25}$$

$$K_{LV} = \varepsilon_{FW}\rho_L\left(\left(1-\frac{S_B}{S}\right)\frac{KK_L}{\mu_L}\frac{R_V T\rho_L}{\tilde{\rho}_V} + \frac{S_B D_B}{S\phi}\frac{\partial\varepsilon_{FW}}{\partial\tilde{\rho}_V}\right) \tag{AII.26}$$

For $S > S_{SSP}$ ($\nabla S_B = 0$. Terms from Eq. AII.19 disappear)

$$K_{LT} = \varepsilon_{FW}\rho_L\left(-\left(1-\frac{S_B}{S}\right)\frac{KK_L R_V\rho_L}{\mu_L}\left(\frac{T}{P_{Sat}}\frac{\partial P_{Sat}}{\partial T} - \left(1+\frac{T}{\rho_L}\frac{\partial\rho_L}{\partial T}\right)\ln\left(\frac{\tilde{\rho}_V R_V T}{P_{Sat}}\right) - 1\right)\right) \tag{AII.27}$$

$$K_{LP} = \left(1-\frac{S_B}{S}\right)\varepsilon_{FW}\rho_L\frac{KK_L}{\mu_L} \tag{AII.28}$$

$$K_{LV} = \varepsilon_{FW}\rho_L\left(1-\frac{S_B}{S}\right)\frac{KK_L}{\mu_L}\frac{R_V T\rho_L}{\tilde{\rho}_V} \tag{AII.29}$$

Figure 1: Benchmark Problem - Plan View on Column Showing Area Analysed by 1-D Model

Figure 2: Results from Original Work (left) (Reproduced from [6]), and Equivalent Results from *Analysis 1*, (right) Showing Profiles of Temperature, Vapour Content per Unit Volume Gas, Vapour Content per Unit Volume Concrete, Liquid Content per Unit Volume Concrete and Gas Pressure, Against Distance from the Exposed Surface After 1s, 600s, 1800s & 3600s of Exposure to Fire (+ & × indicate reported experimental data [6])

Figure 3: Total Mass of Moisture Lost from the Interior of the Discretised Region and Total Mass of Vapour Fluxed through the Boundary, in Time, for Four Model Formulations as Employed in a) *Analysis 1*, b) *Analysis 2*, c) *Analysis 3* & d) *Analysis 4*

Figure 4: Results from *Analysis 1*, *2* & *3* Showing Profiles of Temperature, Gas Pressure, Vapour Content per Unit Volume Gas, Capillary Pressure, Vapour Content per Unit Volume Concrete, Liquid Pressure, Liquid Content per Unit Volume Concrete, Pore Pressure, Free Water Flux and Water Vapour Flux, Against Distance from the Exposed Surface, After 3600s of Exposure to Fire

Figure 5: Results from *Analysis 4*, *5* & *6* Showing Profiles of Temperature, Gas Pressure, Vapour Content per Unit Volume Gas, Capillary Pressure, Vapour Content per Unit Volume Concrete, Liquid Pressure, Liquid Content per Unit Volume Concrete, Pore Pressure, Free Water Flux and Water Vapour Flux, Against Distance from the Exposed Surface, After 7 Days of Exposure to Drying

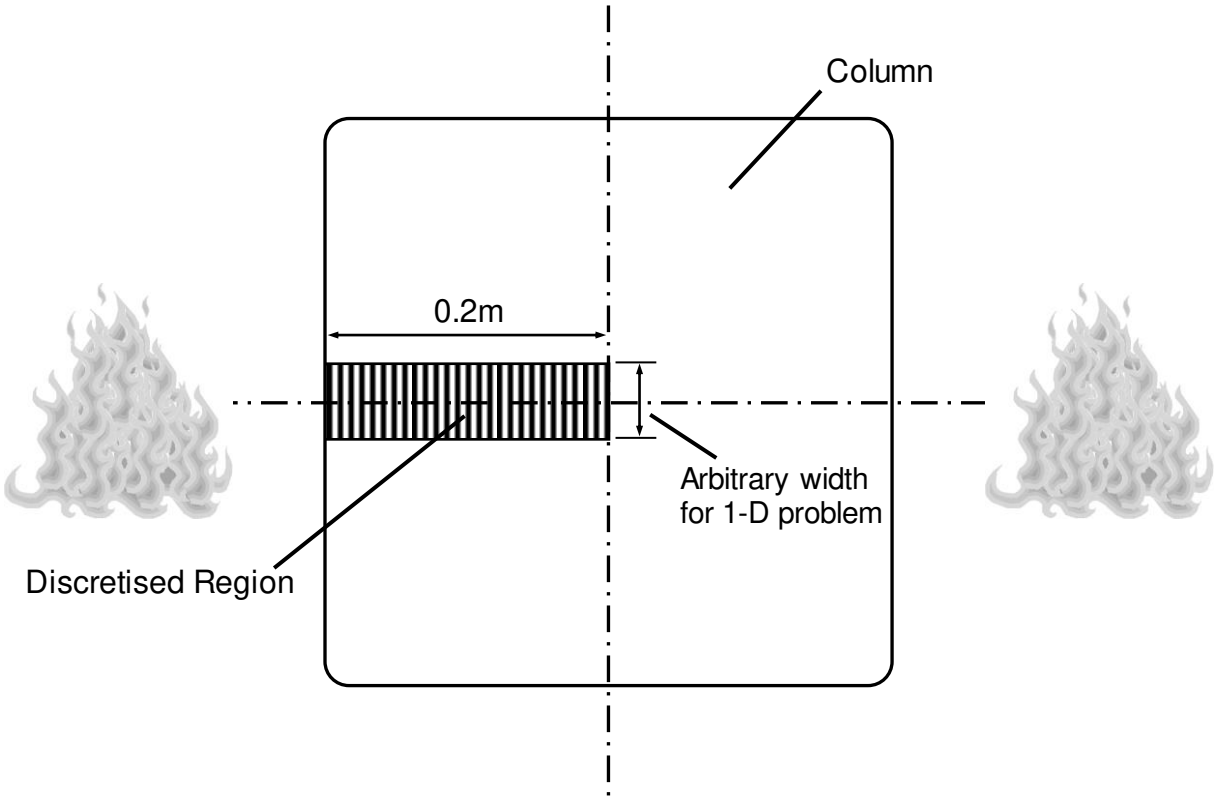
Column
0.2m
Arbitrary width
for 1-D problem
Discretised Region

Figure 1

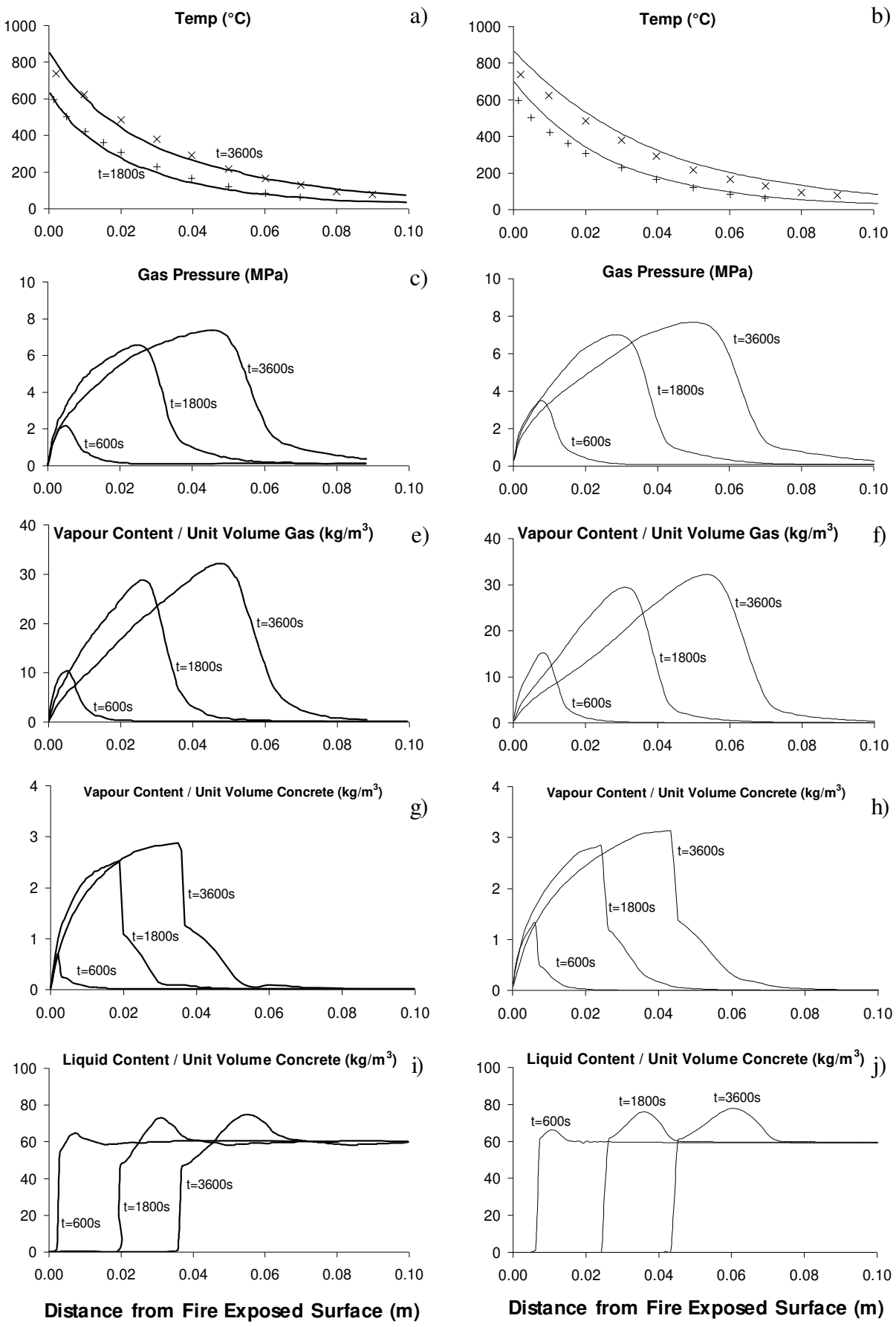
a)
Temp (°C)
1000
800
600
400
200
0
0.00
0.02
0.04
0.06
0.08
0.10
t=3600s
t=1800s
b)
Temp (°C)
c)
Gas Pressure (MPa)
10
8
6
4
2
0
t=3600s
t=1800s
t=600s
Gas Pressure (MPa)
e)
Vapour Content / Unit Volume Gas (kg/m3)
40
30
20
10
0
f)
Vapour Content / Unit Volume Gas (kg/m3)
g)
Vapour Content / Unit Volume Concrete (kg/m3)
4
3
2
1
0
h)
Vapour Content / Unit Volume Concrete (kg/m3)
i)
Liquid Content / Unit Volume Concrete (kg/m3)
100
80
60
40
20
0
j)
Liquid Content / Unit Volume Concrete (kg/m3)
Distance from Fire Exposed Surface (m)
Distance from Fire Exposed Surface (m)

Figure 2

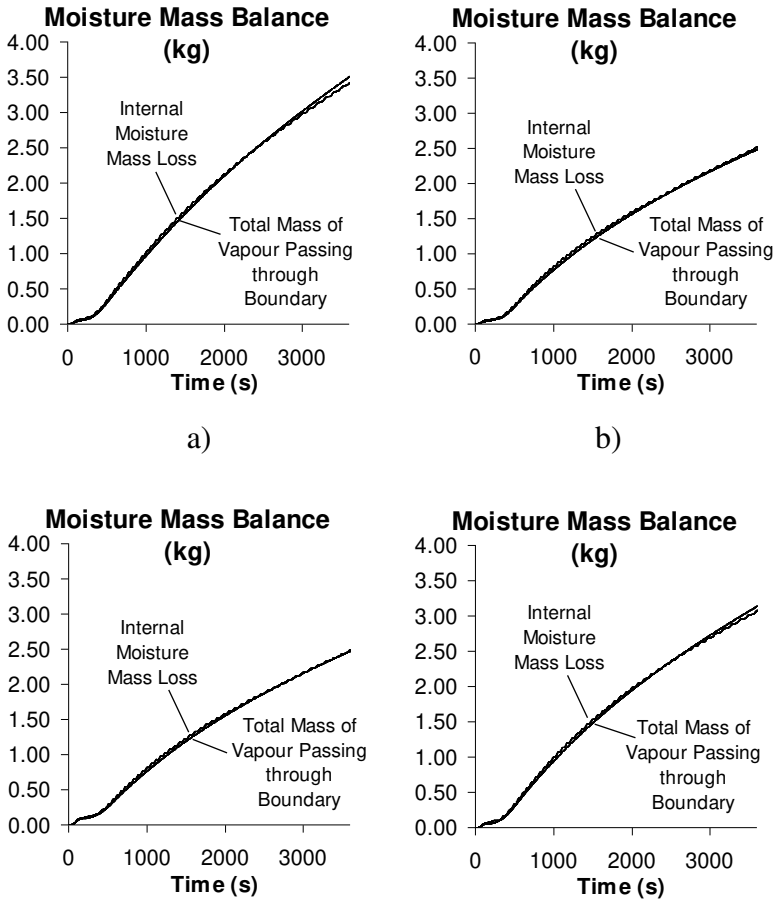
Moisture Mass Balance
(kg)
4.00
3.50
3.00
2.50
2.00
1.50
1.00
0.50
0.00
Internal
Moisture
Mass Loss
Total Mass of
Vapour Passing
through
Boundary
0
1000
2000
3000
Time (s)
a)
Moisture Mass Balance
(kg)
Internal
Moisture
Mass Loss
Total Mass of
Vapour Passing
through
Boundary
Time (s)
b)
Moisture Mass Balance
(kg)
Internal
Moisture
Mass Loss
Total Mass of
Vapour Passing
through
Boundary
Time (s)
c)
Moisture Mass Balance
(kg)
Internal
Moisture
Mass Loss
Total Mass of
Vapour Passing
through
Boundary
Time (s)
d)

Figure 3

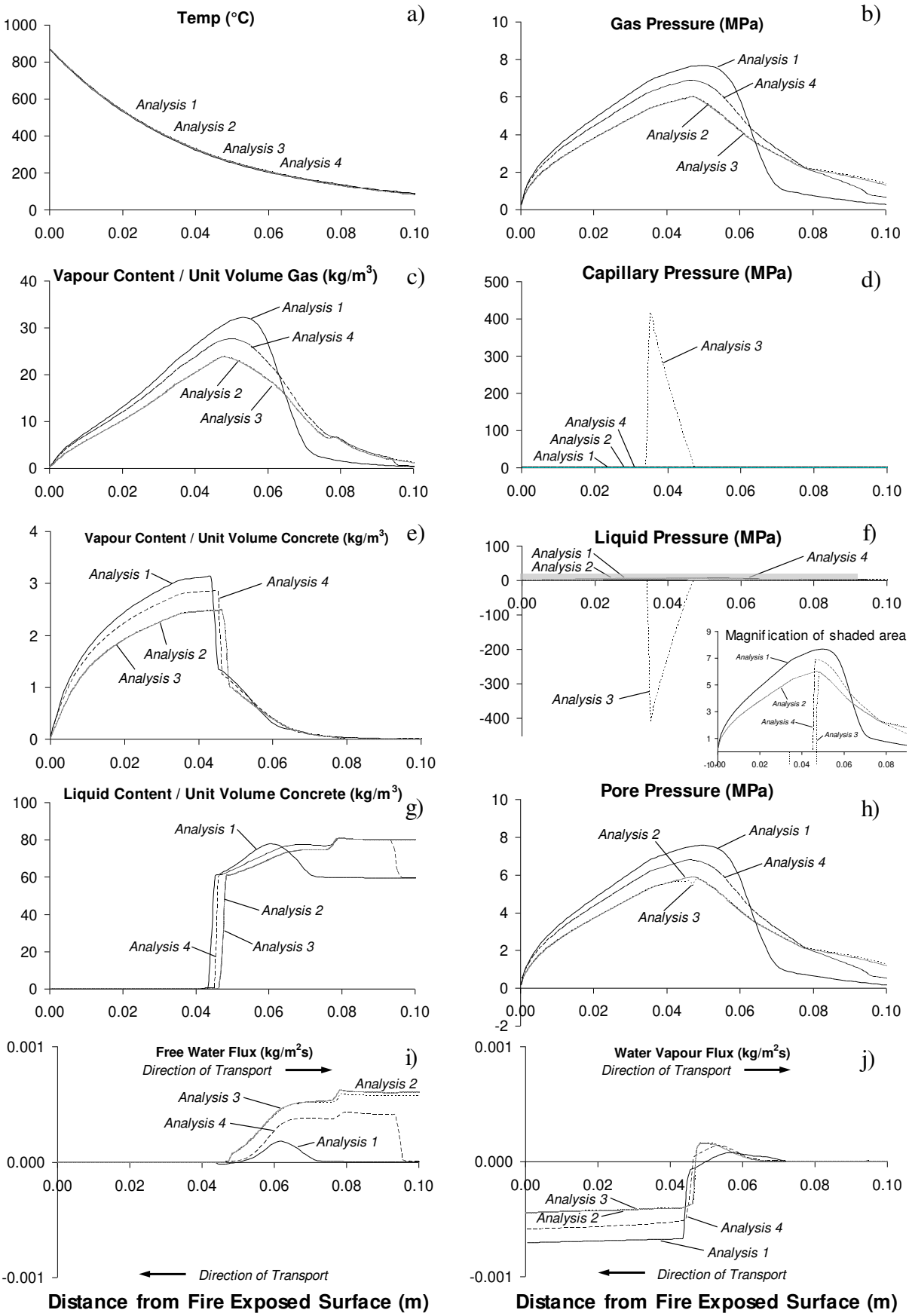
Temp (°C)
a)
Analysis 1
Analysis 2
Analysis 3
Analysis 4
Gas Pressure (MPa)
b)
Vapour Content / Unit Volume Gas (kg/m3)
c)
Capillary Pressure (MPa)
d)
Vapour Content / Unit Volume Concrete (kg/m3)
e)
Liquid Pressure (MPa)
f)
Magnification of shaded area
Liquid Content / Unit Volume Concrete (kg/m3)
g)
Pore Pressure (MPa)
h)
Free Water Flux (kg/m2s)
Direction of Transport
i)
Water Vapour Flux (kg/m2s)
Direction of Transport
j)
Distance from Fire Exposed Surface (m)
Distance from Fire Exposed Surface (m)

Figure 4